Monte Carlo method in optical radiometry

A. V. Prokhorov

Abstract. State-of-the-art in the application of the Monte Carlo method (MCM) to the computational problems of optical radiometry is discussed. The MCM offers a universal technique for radiation transfer modelling based on the stochastic approach. Developments of the original MCM algorithms and software for calculation of effective emissivities of black bodies, absorption characteristics of cavity radiometers and photometric properties of integrating spheres are used for designing advanced optical instruments. The capabilities of the developed software are illustrated by several examples. The techniques of convergence improvement and special time-saving algorithms are outlined.

1. Introduction

The computing problems of optical radiometry relating to radiative-transfer analysis arise at the stage of design of radiometric systems and during the investigation of their metrological characteristics. For these problems, as a rule, it is possible to build a reasonably adequate mathematical model and to write an equation for the radiation-field characteristics in a general form. However, if the system has a sophisticated geometry, or the characteristics of the interaction of the radiation with its elements depend on its conditions of incidence and spectral composition, the solution of the radiative transfer equations by conventional methods becomes extremely difficult and often impossible. In these cases, the MCM can prove to be the only way to solve the problem.

The use of the MCM in optical radiometry is based on a probabilistic treatment of the interaction of radiation and matter. This approach allows the construction of a stochastic model of the system in question and an estimation of its parameters to be made after a large number of stochastic-process realizations. This process may be defined as the passage of a separate ray (or particle – in terms of geometrical optics, the difference is only terminological) all the way from the radiation source to the detector. The accuracy of the solutions obtained is determined by the number of realizations of the stochastic process, and, therefore, progress in computer hardware continues to expand the circle of problems in optical radiometry that can be successfully resolved by using the MCM. These problems include calculation of the

A. V. Prokhorov: Vega International, Inc., 350 Fifth Avenue,
   Suite 6701, New York, NY 10118, USA.
   e-mail: procyon@glasnet.ru

absorption characteristics for the cavities of thermal-radiation detectors and of the effective emissivities of black-body radiators, evaluation of the quality of stray-radiation traps, and modelling of multiple reflections in integrating spheres.

Whatever the algorithm of radiation-transfer statistical modelling, it includes a model of the radiating characteristics of a surface, block of ray tracing, and set of recipes, allowing one to improve the convergence of computing, or to reduce the time needed for these calculations.

The objective of this paper is to analyse the current state of statistical modelling of radiometric systems and their components, describe basic ideas and algorithms of the MCM in optical radiometry, and briefly review the results obtained. As the space available does not permit every aspect of the Monte Carlo method as applied to optical radiometry to be discussed in detail, we only consider several practical implementations and the most interesting results of numerical experiments achieved.

2. Stochastic approach to optical radiation transfer

2.1 Statistical weights

The conventional method of modelling the interaction between radiation and matter can be described as follows. If α and ρ are the absorptivity and reflectivity, respectively, of any opaque body $(\alpha+\rho = 1)$ then, when the ray interacts with the body surface, the program generator of pseudo-random numbers produces the next pseudo-random number η from a sample uniformly distributed on the interval $[0,1]$. If $\eta < \rho$, then the ray reflection by the surface is registered. Otherwise, the absorption is registered, and the ray trajectory is broken off. With low reflectivity values and the need to take into consideration multiple reflections (these are

the conditions that occur inside the cavities of black-body radiators and thermal-radiation detectors), the use of the conventional scheme leads to the overwhelming majority of rays being absorbed, so that they make no contribution to the resulting statistics. The method of statistical weights can provide a good alternative to the conventional scheme. According to this method, a weight $w = 1$ is assigned to each ray before the first interaction. With each reflection, the statistical weight w is multiplied by the reflectivity value ρ. The trajectory ends if the statistical weight w becomes smaller than the pre-specified uncertainty of calculations or if a sufficient number of reflections is achieved. There is a strict proof of the fact that the variation of the result obtained by using the method of statistical weights is always less than that obtained by using the conventional scheme, provided that the number of realizations is the same [1].

In addition to the statistical weight, some other characteristics of simulated radiation can be associated with each ray. For example, in spectral-radiance calculations, the initial spectral radiance $L_{\lambda 0}$ calculated in accordance with the spatial, angular and spectral distributions of source radiance, can be assigned before the ray tracing. The spectral radiance of a ray at any point of the trajectory can be calculated as the product $wL_{\lambda 0}$. If the spectral dependencies are calculated, and the angular distributions of the surface radiating characteristics do not depend on the wavelength λ, it is possible to use a time-saving algorithm by associating a set of wavelengths λ_i and corresponding sets of statistical weights $w_i = w(\lambda_i)$ and spectral radiances $L_i = L_{\lambda 0}(\lambda_i)$, $i = 1, 2, \ldots, n_\lambda$ to each ray. At each reflection, the elements of the array of statistical weights will be multiplied by the reflectivity values at the appropriate wavelength λ_i, and the current values of the spectral radiance are given by $w_i L_i$.

2.2 Models of optical characteristics

The adequacy of the model chosen for the optical characteristics determines the reliability of results obtained by using the MCM in solving optical radiometry problems. The reflection characteristics of any surface are completely determined by its bidirectional reflectance distribution function (BRDF). Because of the difficulty of BRDF measurements and the need to store the large arrays of measurement information, often only spectral dependencies of normal-hemispherical reflectivities are available for opaque bodies. The most frequently used elementary diffuse model assumes that the intensity of radiation reflected by a surface obeys Lambert's cosine law and that the diffuse reflectivity ρ_d does not depend on the radiation angle of incidence. The direction of the reflected ray in a diffuse model is set by the polar angle θ and azimuthal angle φ in a local spherical system of coordinates, the polar axis of which is collinear with the normal to the surface at the ray reflection point. If

η_θ and η_φ are random numbers, then θ and φ can be modelled by the following equations [2]:

$$\sin^2 \theta = \eta_\theta,$$
$$\varphi = 2\pi\eta_\varphi. \tag{1}$$

The choice of a diffuse model for reflected radiation imposes one restriction on the model for emitted thermal radiation: according to the reciprocity theorem and Kirchhoff's law, the emissivity should not depend on the angle of observation.

The second frequently used simple model of reflection is a specular one, which assumes that the specular reflectivity ρ_s is independent of the radiation angle of incidence. The isotropic specular-diffuse model is a superposition of the two previous models. An additional characteristic of the surface is its diffusivity D:

$$D = \rho_d/\rho, \tag{2}$$

where ρ is the directional-hemispherical reflectivity at the same angle of incidence. If the next random number $\eta < D$, then diffuse reflection is assumed; otherwise, specular reflection is assumed.

The anisotropic three-component model is more general and powerful. The retro-component ρ_r, the direction of which coincides with the direction of the incident radiation, is added to the specular and diffuse components of the reflection (see Figure 1). Unlike the previous models, this one allows the components of the reflectivity – diffuse, specular and retro – to be arbitrary functions of the angle of incidence. Let us introduce the following parameter:

$$R = \rho_r/\rho. \tag{3}$$

Reflection is assumed to be diffuse if $\eta < D$, specular if $D \leq \eta \leq 1 - R$, and retro if $\eta > 1 - R$.
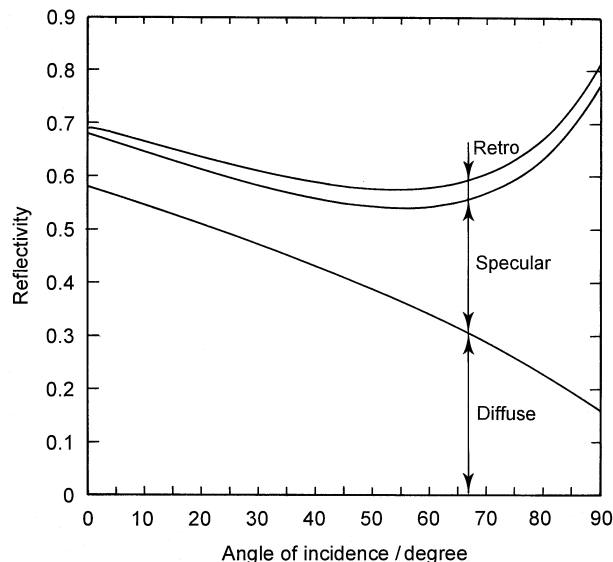
Figure 1. Anisotropic three-component reflectance model.

2.3 Ray tracing

Ray tracing between opaque surfaces is reduced to a consecutive search of points of ray interaction with those surfaces. If ξ_0 is the position vector of the ray starting point, ω is the vector of the ray direction with unit length, and $\Phi(\xi) = 0$ is the equation describing the surface, then it is easy to find the position vector ξ of the point of ray intersection with the surface by solving the following system of equations:

$$\begin{cases} \xi = \xi_0 + \omega t \\ \Phi(\xi) = 0, \end{cases} \qquad (4)$$

where t is a parameter. If the surface is described by a quadratic equation, the extraneous solutions must be eliminated. When the system is formed by several surfaces described by various equations, the system (4) must be solved for each surface and the value of ξ chosen such that, first, it is appropriate for any surface included in the system and, second, it corresponds to the lowest positive value of parameter t.

3. Practical implementation of Monte Carlo algorithms

3.1 Effective absorptivity of cavity radiation detectors

Cavity thermal detectors of radiation are widely used in radiometry and photometry because of the low spectral selectivity of cavity absorption. The effective absorptivity of a cavity depends on its geometrical parameters, the spectral and angular absorption characteristics of the internal walls, and the cavity irradiation conditions. The MCM is an indispensable tool for design, modelling and optimization of cavity radiation detectors.

The paper by Polgar and Howell [3] can be considered to be the first study devoted to the application of the MCM in direct relation to radiometry. Despite their low-performance computer and the imperfection of the proposed algorithm, the authors were able to obtain angular distributions of the radiation reflected by a diffuse conical cavity exposed to oblique irradiation and to calculate the effective absorptivity of the cavity.

Steinfeld [4] has applied the MCM to calculation of the absorptivity of a specular-diffuse, spherical-cavity radiation detector. Mahan and Eskin [5] have described the statistical modelling of radiation-flux distribution over the walls of a cylindro-conical, thermal-radiation detector.

We demonstrate the applicability of the Monte Carlo approach by taking as an example a thermal-radiation detector with a conical cavity irradiated by a collimated radiation beam, with the axis of the beam collinear with the cavity axis and the radius determined by an external diaphragm (Figure 2). The internal surface of the cavity has an absorbing coating
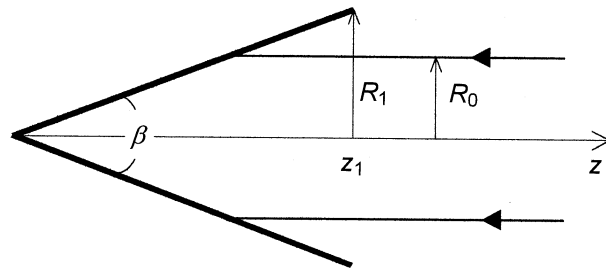
Figure 2. Conical cavity irradiated by collimated beam.

for which we use the isotropic specular-diffuse model of reflection.

We calculate the effective emissivity of the cavity and the distribution of radiation-flux density absorbed by the cavity walls. Such distributions must be taken into account when choosing the location of the temperature sensor and for optimization of the heating-element positioning in case the detector is operated with substitution of the absorbed power by electrical power. For modelling purposes, we divide the cavity surface into ring zones of equal area and then sum up the statistical weights of the absorption in each zone after multiple reflections of the ray in the cavity.

Relative distributions of the absorbed-flux density along the generatrix of the conical cavity are shown in Figure 3 for $R_0 = 0.75$, $R_1 = 1$, $\beta = 15°$, with the absorptivity of the internal walls $\alpha = 0.5$ and for various values of diffusivity D. In numerical experiments, 10^6 rays were used, with their traces stopped if the statistical weight became less than 10^{-4}. The cavity generatrix was divided into 200 ring zones.
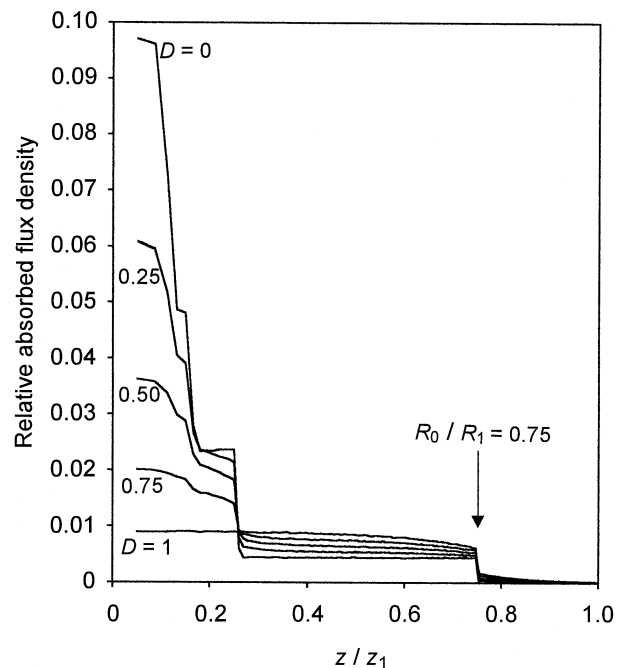
Figure 3. Relative distributions of absorbed-flux density along the generatrix of a $15°$ conical cavity for (see Figure 2) $R_0/R_1 = 0.75$ and absorptivity $\alpha = 0.5$.

For $D = 1$ we obtain ideal diffuse reflection, yielding a smooth distribution of absorbed fluxes over the initially irradiated zone and "tails" at the edges of that zone due to the multiple reflections. After the appearance of the specular component, the distribution over the initially irradiated zone turns out to be essentially non-uniform. For the purely specular reflection, the distribution of absorbed fluxes represents a step function.

As elementary geometric considerations show, the boundary position of the first step is determined by the penetration depth of the extreme beam rays in the cavity. The height of this step is determined by absorption of the rays at the first and last (12th) reflections. The steps of the distribution located near the cone vertex are formed by absorption of combinations of rays which have undergone different numbers of reflections. The appearance of the reflection diffuse component smoothes out the stepped profile of the distribution. The "tails" of the distributions in the area not subjected to the initial irradiation are observed for all non-zero values of D. They become smaller as the reflection from the cavity walls approaches a perfectly specular character.

Simple summation of the statistical weights absorbed by the whole cavity surface (or even calculation of the statistical weights of rays leaving the cavity after multiple reflections) enables one to calculate the effective absorptivity (or effective reflectivity) of the cavity. Figure 4 shows the normal effective absorptivity of a 15° conical cavity as a function of the absorptivity of the internal wall coating for various values of diffusivity D.
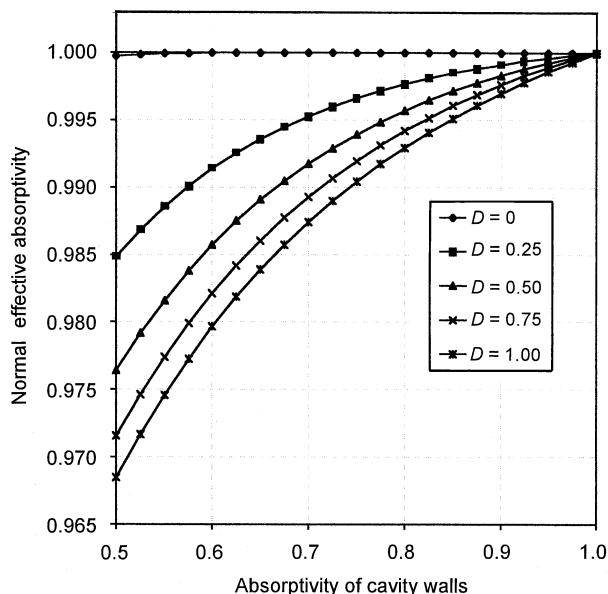
Figure 4. Normal effective absorptivity of a specular-diffuse conical cavity as a function of absorptivity of cavity walls for various values of diffusivity D and for $R_0/R_1 = 0.75$.

3.2 Black-body radiators

For some considerable time, cavity radiators have been successfully used as reference sources whose radiation characteristics can be calculated by using the Planck and the Stefan-Boltzmann laws. Generally, the effective emissivity depends on the cavity geometry, the temperature distributions and optical characteristics of the cavity internal surface, and the observation conditions. Effective emissivity calculations present a non-trivial problem even in the case of cavities having elementary geometrical forms with diffuse internal surfaces. For cavities of a complex form with surfaces partially shading each other, the MCM can be the most suitable tool for computing the radiation characteristics.

Heinisch et al. [6] have used the MCM to calculate the hemispherical emissivity of a diffuse conical cavity with a flat lid with an uncertainty of about 0.0001. To accelerate the convergence, they applied analytical integration to calculate the radiant energy leaving the cavity at each act of emission or reflection. The algorithm employed allowed them to take into consideration the arbitrary temperature distribution along the cavity walls, but it was impossible to use it for calculation of the directional radiation characteristics.

Ono [7, 8] has obtained important results for the directional radiative characteristics of isothermal specular-diffuse cavities used as reference sources of infrared radiation. By applying the generalized Kirchhoff's law and the reciprocity theorem in the computing algorithm, Ono studied cylindro-conical cavities, a cylindrical cavity with a lateral hole, and a system formed by a flat target and a hemispherical mirror. Chu et al. [9] have applied a similar algorithm to parametrical calculation of the effective emissivity of a black body having cylindrical lateral walls and an internal conical bottom in specular-diffuse reflection conditions.

All the works listed above used the conventional Monte Carlo technique which prescribes the truncation of a trajectory in the case of ray absorption by the cavity wall. In a series of studies [10-12], algorithms based on the method of statistical weights were described and successfully used for statistical modelling of the effective emissivities of cavities formed by a number of coaxial cylindrical and conical surfaces. In the effective emissivity calculations, the optical reciprocity theorem and the technique of inverse ray tracing were used. A ray with statistical weight equal to unity was directed from the point of observation into a cavity. Its history was traced until it left the cavity after reflections from the walls, or until its statistical weight became less than the given value. We can consider the last point of reflection to be a birth point of a ray propagating in the opposite direction. By choosing the reference temperature T_{ref}, and analysing the history of a large number of rays, n, one can evaluate the

spectral effective emissivity of the cavity for the given observation conditions and reference temperature:

$$\varepsilon_{\lambda e}(\lambda, T_{\mathrm{ref}}) =$$

$$\frac{\exp\left(\dfrac{C_2}{\lambda T_{\mathrm{ref}}}\right) - 1}{n} \sum_{i=1}^{n}\sum_{j=1}^{m_i} \frac{\varepsilon_j}{\exp\left(\dfrac{C_2}{\lambda T_j}\right) - 1} \prod_{k=1}^{j-1} \rho_k, \tag{5}$$

where m_i is the number of ray reflections in the i-th trajectory; λ is the wavelength; C_2 is the second constant in Planck's law and ε_j, ρ_j and T_j are the emissivity, reflectivity and temperature, respectively, at the j-th point of reflection.

Figure 5 presents the calculated normal spectral effective emissivities ε_e of the pyrographite black body BB3200pg [13] with the temperature at the centre of the base fixed at 3000 K; several temperature distributions are considered, with temperature increasing linearly in each case towards the edge of the base. A linear decrease in temperature to 2950 K was set along the cylindrical generatrix towards the isothermal lid. The cylindrical radiating cavity has a length of 200 mm and diameters of the cavity and the aperture of 37 mm and 22 mm, respectively. The same set of 10^5 trajectories was used for modelling all six spectral curves. The curve corresponding to the isothermal cavity lies between the curves obtained for a temperature increase towards the bottom edge, equal to 1.5 K and 3 K, because the effective radiation – consisting of the emitted thermal radiation of the non-isothermal bottom for a temperature increase of about 2 K and reflected radiation of the non-isothermal lateral walls – closely
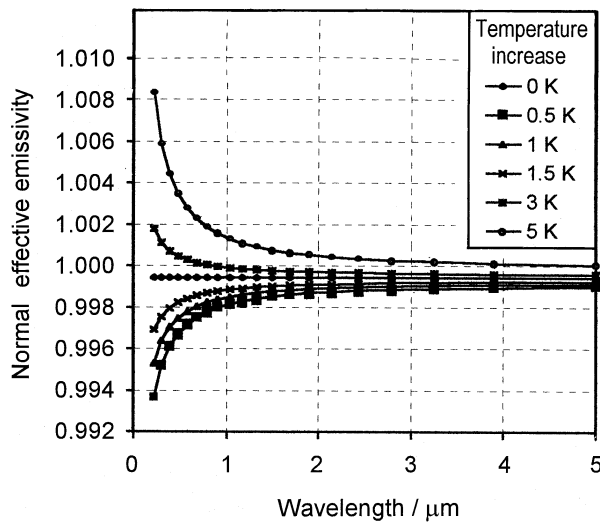
Figure 5. Normal spectral effective emissivities of black body BB3200pg for various values of linear temperature increase towards the bottom edge. Reference temperature is the temperature at the centre of the base (3000 K). The temperature decreases along the lateral walls towards the aperture, which is isothermal at 2950 K.

matches the radiation of the isothermal cavity at the temperature $T_{\mathrm{ref}} = 3000$ K.

Test calculations for diffuse cavities [14-17] have shown that a relative uncertainty $\Delta\varepsilon_e/\varepsilon_e < 10^{-4}$ for $\varepsilon_e > 0.99$ is reached after tracing between 10^4 and 5×10^4 rays.

The MCM can be used for exact calculation of the irradiance produced by an arbitrary black-body radiator under given conditions (see Figure 6). For this purpose, ray tracing through the external aperture into the cavity is performed from a point located on the observation plane. The radiation emitted by the external surface of the cavity lid is assumed to be negligible. The spectral irradiance of the point on the observation plane is computed as

$$E_\lambda = \frac{\pi R_0^2}{n} \sum_{i=1}^{n} \frac{L_{\lambda i} V_i \cos^2\theta_i}{l_i^2}, \tag{6}$$

where $L_{\lambda i}$ is the radiance of the ray at the cavity aperture; l is the distance between the observation point and the point of ray intersection with the external aperture plane; θ_i is the angle between the i-th ray and the optical axis of the system; V_i is the vignetting function, which is equal to 1 if the ray hits the cavity aperture during ray tracing from the observation point through the external aperture; otherwise, it equals zero.
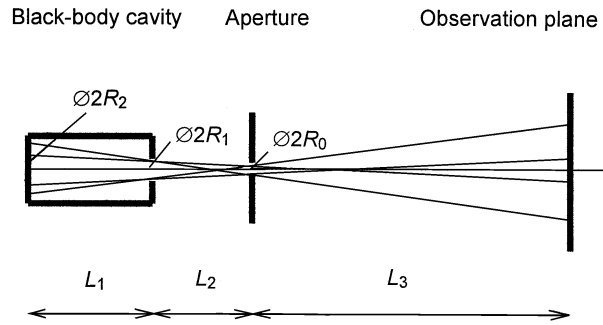
Figure 6. Scheme for calculation of irradiation distribution.

Figure 7 shows the spatial distributions of spectral irradiance at a wavelength of 650 nm, produced by a black body with $R_1 = 7.5$ mm, $R_2 = 10$ mm, $L_1 = 200$ mm and the wall emissivity $\varepsilon = 0.9$. The cavity walls were assumed to be specular-diffuse with $D = 0.9$. Other geometrical parameters of the system are as follows: $R_0 = 2.5$ mm, $L_2 = 200$ mm, and $L_3 = 500$ mm. The first curve corresponds to the cavity having a constant temperature of 2500 K, while the second and third curves relate to the cavities with an isothermal bottom and a linear temperature drop to 2475 K and 2450 K, respectively, along the cylindrical generatrix towards the isothermal lid. Even for the case of the isothermal cavity, the irradiance distribution differs from that of the isothermal diffuse disk replacing the cavity aperture. This is explained by the higher effective emissivity of the part of the cylindrical wall in close proximity to the bottom in
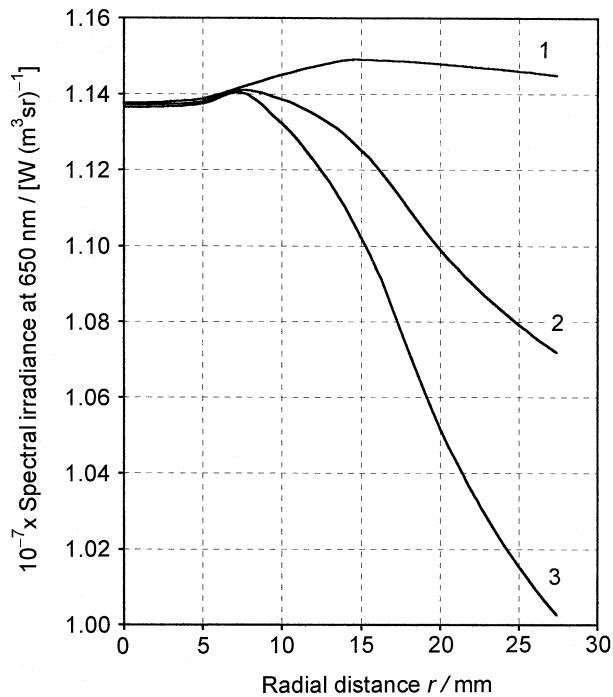
Figure 7. Spatial distribution of spectral irradiance at 650 nm for (see Figure 6) $R_0 = 2.5$ mm, $R_1 = 7.5$ mm, $R_2 = 10$ mm, $L_1 = L_2 = 200$ mm, $L_3 = 500$ mm. Curve 1, cavity is isothermal at 2500 K; curve 2, bottom is isothermal at 2500 K, temperature decreases linearly along lateral walls to 2475 K at the intersection with the isothermal flat lid; curve 3, bottom is isothermal at 2500 K, temperature decreases linearly along lateral walls to 2450 K at the intersection with the isothermal flat lid.

comparison with the effective emissivity of the bottom, caused by the specular component of reflection. The temperature gradient along the lateral cylindrical wall leads to a sharp decrease in the spectral irradiance away from the optical axis (curves 2 and 3).

3.3 Integrating spheres

An extensive area for MCM application is the modelling of integrating spheres: for reflectivity and transmittance measurements [18], for use as a calibrated diffuser [19], for flux comparison of various sources of radiation [20], for building large-aperture uniform sources, etc. Numerical modelling of integrating spheres becomes even more important in the realization of the lumen based on a black-body source and a spherical integrator of the luminous flux [21].

The main difficulty in application of the MCM in the modelling of integrating spheres is as follows. The coating of the internal walls of the sphere has, as a rule, a reflectivity very close to 1. This leads to extremely slow convergence of the computing process; to obtain three to four decimal digits in the computed illuminance of sphere walls, one has to trace several hundred successive reflections.

However, the sphere has an important property that allows the calculation time to be reduced. If a point on the sphere wall reflects in accordance with Lambert's cosine law, then the sphere internal surface has constant illuminance. This fact makes it possible to avoid use of the conventional modelling sequence, employing generation of two random numbers η_θ and η_φ, calculating angles θ and φ in accordance with (1), calculating the vector coordinates in the local Cartesian coordinate system, transforming to the global Cartesian system, and searching for the point of intersection between the reflected ray and the sphere by solving the system of equations (4). Instead, the random point uniformly distributed over the spherical surface is generated by a known algorithm. The line connecting this point with that of the previous reflection will determine the direction of the diffuse reflection. Acceleration of the convergence of the result for computation of the photometric head illuminance can be achieved by calculating the diffuse angle factors [2] from the point of ray reflection to the radiation detector except where it is shaded by a baffle.

3.4 Other radiometric applications of the Monte Carlo method

3.4.1 Stray-light analysis

The MCM is successfully used in the optimization of various stray-radiation traps [12, 22, 23]. There are commercially available, MCM-based, software products for analysing the stray radiation in optical systems (ASAP, Breault Research Organization; GUERAP V, Lambda Research Corp.). The most advanced programs allow simulation of the real BRDF by splitting each reflected ray into a large number (10^2 to 10^4) of secondary rays. Each secondary ray contributes to the characteristics of radiation calculated from the BRDF of the reflecting surfaces. As a result, the trajectories of rays become tree-like, and significant time on top-performance computers is required for their sequential tracing.

3.4.2 Transmittance of glass filters

Exact calculation of the spectral transmittance of composite glass filters irradiated by non-collimated radiation beams (for example, in the presence of a diffuser) can be successfully performed by the MCM-based code. Thus, it is easy to perform ray tracing taking into account the reflections at the interface of glasses with diverse refractive indices.

3.4.3 Overall simulation of radiometric and photometric systems

The MCM allows modelling of the most sophisticated radiometric systems [12] by coordinating the entrance parameters of the subsequent part of the system with the target parameters of the previous one. The system can

have multiple sources and detectors of radiation with scattering, refracting and reflecting elements placed between them. A single model implemented in a computer code can be used repeatedly for evaluation of the system's performance for various initial data sets. The block structure makes it easy to model a system even after the addition of new components; the entire unit is then readily analysed.

4. Further development prospects

Significant progress in the complexity of soluble problems and in the accuracy of the results obtained has been achieved over the three and a half decades of the application of the MCM to optical-radiometry problems. This progress, however, is to be attributed more to the growth of computer performance than to improvements in computing algorithms. Analysis of the present state of radiometric applications for the MCM has shown that researchers in this area should focus on the following important and still unsolved problems:

(a) Development of correct methods to describe the experimental BRDF of real materials by a simplified reflectance model (isotropic specular-diffuse or anisotropic three-component model).

(b) Development of direct (without trajectory splitting) methods to model directions of relected rays to match the given BRDF.

(c) Development of convergence-acceleration methods for algorithms to model multiple reflections in systems with surfaces having a reflectivity very close to 1.

(d) Creation of advanced MCM algorithms leaving the framework of geometrical optics by inclusion of diffraction [23] and polarization effects [24].

(e) Use of parallel computing systems and appropriate algorithms to increase the modelling efficiency for optical-radiometry problems.

The experience of intensive use of the MCM in adjacent areas – such as radiative heat transfer, atmospheric optics, and computer image modelling – can be extremely useful for resolving these problems. We have every reason to believe that use of the MCM technique will allow the most important problems of optical radiometry associated with radiation transfer to be handled within the next ten or fifteen years.

References

1. Mikhailov G. A., *Optimization of weighted Monte Carlo methods*, Berlin, Springer-Verlag, 1992, 225 p.

2. Siegel R., Howell J. R., *Thermal radiation heat transfer,* Washington, D.C., Hemisphere Pub., 1992, 652 p.

3. Polgar L. G., Howell J. R., NASA Technical Note *D-2904*, 1965, 37 p.

4. Steinfeld A., *Int. J. Heat Mass Transfer*, 1991, **34**, 1895-1896.

5. Mahan J. R., Eskin L. D., In *Proc. 4th Conf. Atmospheric Radiation,* 1981, Toronto, 181-186.

6. Heinisch R. P., Sparrow E. M., Shamsundar N., *J. Opt. Soc. Am.*, 1973, **63**, 152-158.

7. Ono A., *J. Opt. Soc. Am.*, 1980, **70**, 547-554.

8. Ono A., *Int. J. Thermophys.*, 1986, **7**, 443-453.

9. Chu Z., Dai J., Bedford R. E., In *Temperature: Its Measurement and Control in Science and Industry*, Vol. 6 (1) (Edited by J. F. Schooley), New York, American Institute of Physics, 1992, 907-912.

10. Sapritsky V. I., Prokhorov A. V., *Metrologia*, 1992, **29**, 9-14.

11. Sapritsky V. I., Prokhorov A. V., *Appl. Opt.*, 1995, **34**, 5645-5652.

12. Prokhorov A. V., Martin J. E., *Proc. SPIE,* 1996, **2815**, 160-168.

13. Sapritsky V. I., Khlevnoy B. B., Khromchenko V. B., Lisiansky B. E., Mekhontsev S. N., Melenevsky U. A., Morozova S. P., Prokhorov A. V., Samoilov L. N., Shapoval V. I., Sudarev K. A., Zelener M. F., *Appl. Opt.*, 1997, **36**, 5403-5408.

14. Bedford R. E., Ma C. K., *J. Opt. Soc. Am.*, 1974, **64**, 339-349.

15. Bedford R. E., Ma C. K., *J. Opt. Soc. Am.*, 1975, **65**, 565-572.

16. Bedford R. E., Ma C. K., *J. Opt. Soc. Am.*, 1976, **66**, 724-730.

17. Bedford R. E., Ma C. K., Chu Z., Sun Y., Chen S., *Appl. Opt.*, 1985, **24**, 2971-2980.

18. Hanssen L. M., *Appl. Opt.*, 1996, **35**, 3597-3606.

19. Growther B. G., *Appl. Opt.*, 1996, **35**, 5880-5886.

20. Prokhorov A. V., Sapritsky V. I., Mekhontsev S. N., *Proc. SPIE*, 1996, **2815**, 118-125.

21. Sapritsky V. I., Khlevnoy B. B., Shapoval V. I., Prokhorov A. V., Stolyarevskaya R. I., In *Proc. 23rd Session CIE*, 1995, New Delhi, 83-86.

22. Waluschka E., Qiu S.-Y., Godden G. D., *Proc. SPIE*, 1996, **2864**, 350-360.

23. Likeness B. K., *Proc. SPIE*, 1977, **107**, 80-88.

24. Lo C., Palmer B. J., Drost M. K., Welty J. R., *Numerical Heat Transfer, Part A (Applications),* 1995, **27**, 129-142.